CCFE
CULHAM CENTRE FOR FUSION ENERGY

UK Atomic Energy Authority

UKAEA-CCFE-CP(23)38

S. Omole, A J G Lunt, S Kirk, A Shokrania

Surface and subsurface evaluation in conventional machining of commercially pure tungsten

Surface and subsurface evaluation in conventional machining of commercially pure tungsten

S. Omole, A J G Lunt, S Kirk, A Shokrania

This paper has been submitted to
6th CIRP Conference on Surface Integrity, Lyon, France, 8-10 June 2022

Available online at www.sciencedirect.com

ScienceDirect

Procedia CIRP 00 (2021) 000–000

www.elsevier.com/locate/procedia

6th CIRP Conference on Surface Integrity

Surface and subsurface evaluation in conventional machining of commercially pure tungsten

Samuel Omole[a,*], Alexander J G Lunt[a], Simon Kirk[b], Alborz Shokrani[a]

[a]*Department of Mechanical Engineering, University of Bath, Bath, BA2 7AY, United Kingdom*
[b] *United Kingdom Atomic Energy Authority, Culham Science Centre, Abingdon, OX14 3DB,United Kingdom*

* Corresponding author. Tel.: +44-1225-38-6588; fax: +44-1225-3865. *E-mail address:* so444@bath.ac.uk

Abstract

The high ductile-to-brittle transition temperature (DBTT) of tungsten combined with its high hardness make machining incredibly difficult. These properties typically result in the poor-quality machined surfaces and short tool life. In this study, TiAlN coated carbide tools with different rake angles (8°, 10° and 12°) were tested in conventional milling at different cutting speeds (60 m/min, 100 m/min and 150 m/min) and preheating temperatures (400°C, 500°C and 600°C). The resulting surfaces were examined, and the assessment of relevant surface/sub-surface features was performed to understand the impact of deformation. Surface examinations revealed the presence of ductile and brittle fracture regions. The study showed that machining at 60 m/min produced the best performance with the 12° rake resulting in the longest tool life while preheating has no effect. Further assessment of the tool wear at the optimized cutting speed revealed that the tool nose was the location of principal structural weakness where additional strengthening could enhance tool life.

Keywords: tungsten; machining; surface integrity

1. Introduction

The exceptional strength and high temperature characteristics of tungsten make it the material of choice for extreme environment components. Recent decades have seen a significant increase in its use within the nuclear fusion industry, particularly within divertor assemblies and reactor walls [1]. However, the same properties which have caused its widespread adoption make machining incredibly difficult. The high DBTT (at least 200°C) is also a challenging aspect of the material [2]. Improvements in machinability will alleviate current manufacturing challenges and benefit various sectors where tungsten parts are used.

The limited research on machining of tungsten is focused on tool performance. Rapid tool wear has been reported within these studies alongside the underlying wear mechanism. Zhong et al. [3] observed that the wear (mostly flaking) is more severe on the rake face compared to the flank of the polycrystalline diamond (PCD) tool used during micro cutting. Legutko et al. [4] reported on the abrasion-dominated wear of various tools used during turning with whisker reinforced alumina ceramics providing the most resistance. Olsson et al. [5] tested various tool types in turning and found TiAlN-TiSiN coated carbide and PCD as the best options, although PCD was superior. Abrasion and diffusional dissolution were identified as the main wear mechanisms. Olsson et al. [6] investigated the performance of different machining methods including cryogenic cooling, high pressure cooling, induction assisted heating, dry and flood cooling. Cryogenic cooling was found to provide the most improvement to tool life despite the significant level of adhesion.

It is evident from the review of these studies that they are concentrated on the turning operation with limited emphasis on the analyses of the surface integrity. This paper, on the other hand, is based on the milling operation and aims to fill the gap in this area. The selection of suitable milling parameters is investigated whilst considering the effect of preheating on machinability.

2. Experimental procedure

End milling of 99.99% pure dense tungsten was performed on a vertical CNC milling machine with a 13 kW spindle. The experiments involved different rake angles, cutting speeds and workpiece temperatures using a TiAlN coated solid carbide tool with climb milling strategy. All tools have two teeth and identical geometries except for the rake angle as shown in Table 1. The tungsten workpiece is a block of dimension 20 X 20 X 40 mm. The cutting parameters used in this study are listed in Table 1 including the preheating temperatures used. Preheating was achieved through conductive heating of the workpiece using two 750 W cartridge heaters as shown in the set-up in

Fig. 1. The temperature was maintained throughout the experiment using a closed loop thermocouple-based sensing and control element. The tool bending moment was measured using a SPIKE® sensory tool holder with a sample rate of 2.5 kHz. Optical microscopy observations of the machined surfaces were performed using a Keyence VHX-6000 digital microscope. Cross-sections of the machined sample (sectioned perpendicular to the direction of feed) were mounted in resin, polished and etched to reveal the grain structures. These subsurface grains were examined through backscattered-electron imaging.

Table 1. Cutting and preheating temperature parameters

Parameter	Value
Feed/tooth/revolution (mm)	0.03
Cutting speed (m/min)	60, 100, 150
Axial depth of cut (mm)	3
Radial depth of cut (mm)	3
Rake angle (°)	8, 10, 12
Tool radius (mm)	6
Preheating temperature (°C)	400, 500, 600

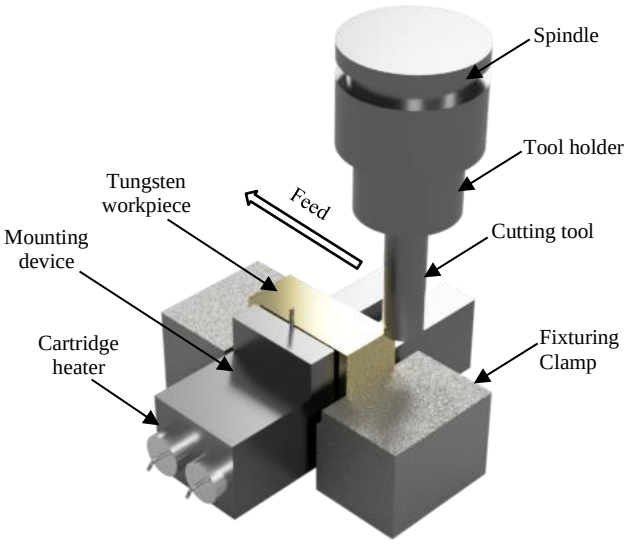

Fig. 1 Experimental set-up showing the mounting device and cartridge heaters used for preheating

3. Results and discussion

3.1. Bending moment signals and tool wear

The impact of the rake angle on the resultant bending moment is shown in Fig. 2(c) where the signals decrease with increase in the rake angle, with the 12° rake being the lowest. On average, the resultant bending moment decreases by 21% and 35% when the rake angle increases from 8° to 10° and 8° to 12° respectively.

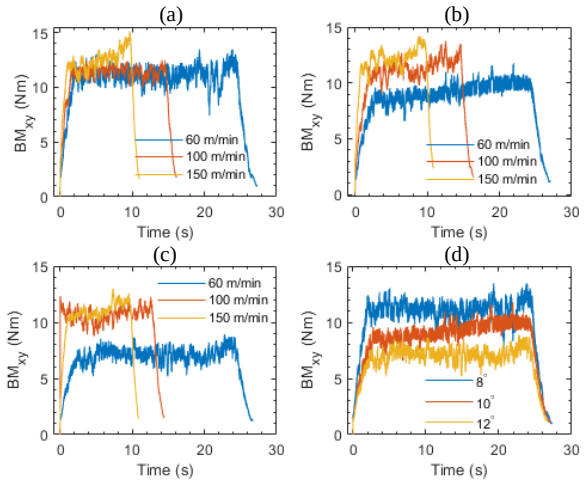

Fig. 2. Resultant bending moment plots showing the impact of cutting speed at (a) 8° rake; (b) 10° rake; (c) 12° rake; and (d) impact of rake geometry at 60 m/min

The influence of the cutting speed was also observed through the plots in Fig. 2(a), (b) and (c). Overall, the bending moment increases with increase in cutting speed. There is also no noticeable difference in the bending moment signals at the start of the cutting shown in Fig. 2(a) for the 8° rake angle regardless of the cutting speed. However, the signal at 60 m/min separates itself at 10° and even better at 12° (Fig. 2(b) and (c)). Fig. 2 suggests that a higher rake angle and lower cutting speed is required for machining tungsten, with the positive effect of the low cutting speed being more pronounced with increase in the rake angle.

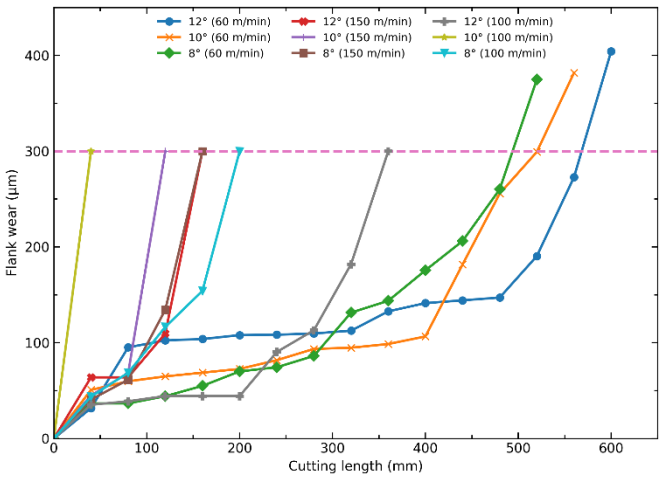

Fig. 3. Tool wear progression for a combination of rake angle and cutting speed.

The effect of an increase in the bending moment is the degradation of the tool through wear. The wear progression for each tool is shown in

Fig. 3 with the 60 m/min cutting speed showing longer tool life compared to the higher cutting speeds. For quantification purpose, the tool lives are 327 s, 352 s and 377 s for the 8°, 10°

and 12° rake angles respectively. These support the bending moment signal observations in Fig. 2. At 150 m/min, a maximum tool life of 40 s (with the 8° and 12° tool) was achieved while it was 136 s with the 12° tool when machining at 100 m/min. Preheating at 400 °C and 500 °C resulted in similar tool lives of 301 s compared to 251 s at 600 °C. Further comparison with the dry machining condition at 60 m/min indicates an inferior tool life.

Post-machining tool wear observations (Fig. 4) show that the tool wear is not concentrated on the flank face. Rather, there are evidence of chipping, predominantly in the secondary flank face and wear in the nose regions, regardless of the rake angle. This chipping could be due to localized mechanical stresses. Edge chipping is also noticeable in all cases which also be attributed to mechanical stresses. The nose wear can be a result of abrasion between the nose and the workpiece. This wear mode at the contact with newly machined surfaces can also be responsible for increase in the surface roughness. The flank wear is concentrated at the depth of cut for both the 8° and 10° cutting tools. However, it is more distributed for the 12° rake angle (Fig. 4(e) and (f)) as a more uniform profile up to the adjoining nose region can be seen. The hardness of the tungsten workpiece and the resulting abrasion explains the flank wear.

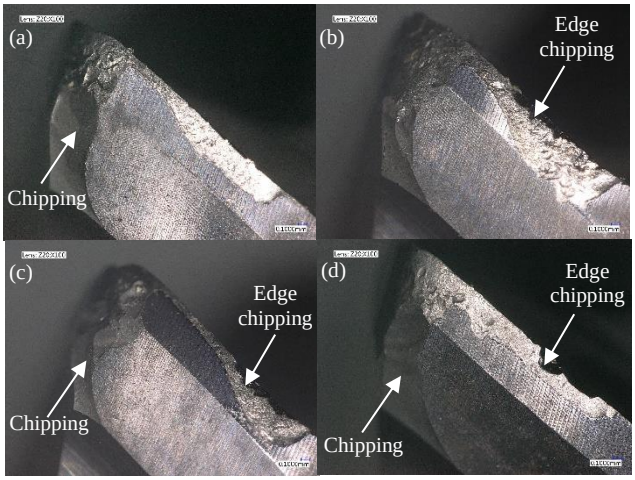

Fig. 4. Post-machining tool wear at 60 m/min for (a) 8° rake angle (teeth 1); (b) 8° (teeth 2); (c) 10° rake angle; (d) 12° rake angle

Fig. 5 shows the wear modes due to higher cutting speeds. Severe damages can be seen on the flank faces up to the depth of cut at 150 m/min for all rake angles. This damage is instantaneous and could be attributed to severe abrasive and thermal effect at higher cutting speeds. Post machining microscopic analysis of the machined surfaces show evidence of severe plastic deformation up to the depth of cut. These show that the adverse effect of higher cutting speed is not only on the cutting tool but also on the workpiece.

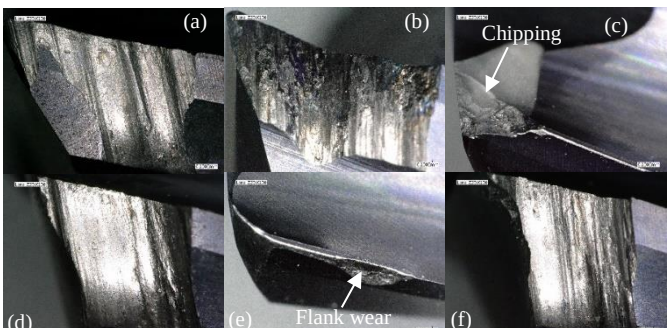

Fig. 5 Post-machining wear observations at higher cutting speeds for (a) 8° at 100 m/min; (b) 8° at 150 m/min; (c) 10° at 100 m/min; (d) 10° at 150 m/min; (e) 12° at 100 m/min; (f) 12° at 150 m/min

The wear modes at 100 m/min are more varied as Fig. 5((a), (c) and (e)) show. Similar damage at 150 m/min can be seen on the tool with 8° rake angle. However, severe chipping of the flank and rake faces can be observed on the 10° rake tool. Flank wear is evident on the 12° tool with more uniform wear on the rake face closer to the cutting edge.

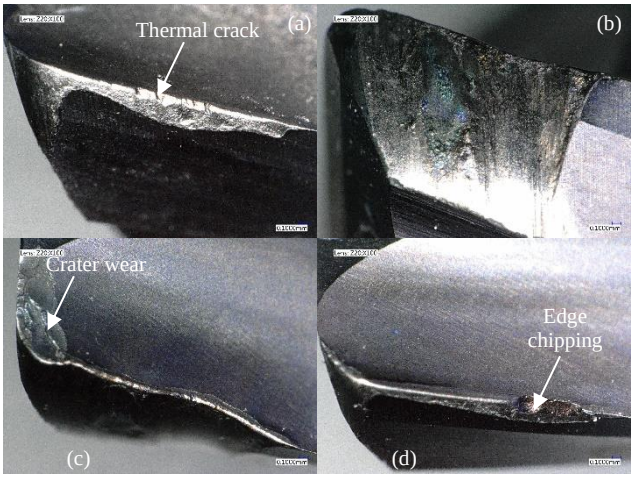

Fig. 6. Post-machining wear observations due to preheating at (a) 400°C; (b) 500°C (flank side); (c) 500°C (rake side); (d) 600°C

The tool wear modes due to preheating are shown in Fig. 6 where thermal cracks (due to interrupted cuts), crater and edge chipping can be observed. Additionally, the tool at 500 °C is more severely damaged despite the cutting speed being 60 m/min. It is also obvious that the nose chippings observed during the dry machining conditions in Fig. 4 are absent.

3.2. Surface quality and damage

For reference, the surface roughness (R_a) of tungsten using TiAlN-TiSiN coated carbide tool was reported by Olsson et al. [5] to be within 1-1.5 μm. In this section, the effect of both cutting speed and rake angle on the surface roughness was evaluated and investigated in terms of R_a and R_z parameters as shown in Fig. 7. A one-way ANOVA test was used to test for statistically significant difference between the means of the different groups. The null hypothesis with significance level of 0.05 was chosen. Multiple pairwise-comparison (using Tukey Honest Significant Difference) was also used to aid the test.

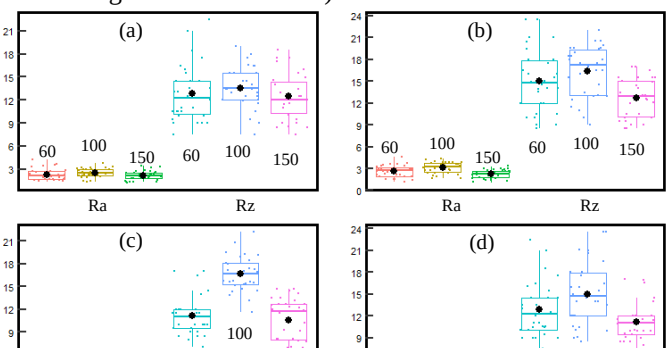

Fig. 7. Surface roughness plots due to effect of cutting speed (in m/min) for (a) 8°; (b) 10°; (c) 12° and (d) due to the rake angle at 60 m/min

Fig. 7(a), (b) and (c) show the effect of the cutting speed for the 8°, 10° and 12° rake angles, respectively, at 60, 100 and 150 m/min. For the 8° rake angle, average R_a values are 2.3 µm, 2.52 µm and 2.19 µm compared to 2.60 µm, 3.11 µm and 2.24 µm for 10° and 2.01 µm, 3.32 µm and 1.93 µm for 12°. The cutting speed does not have a significant influence on the surface roughness for the 8° rake angle. However, for 10°, there is significant impact except between 60 and 150 m/min for R_a and 60 and 100 m/min for R_z. There is also impact due to the cutting speed at 12° except between 60 and 150 m/min. Overall, the deduction from the statistical test is that the cutting speed influences the surface roughness.

Fig. 7(d) shows the average R_a values as 2.3 µm, 2.60 µm and 2.01 µm for 8°, 10° and 12° rake angles respectively while corresponding R_z values are 12.85 µm, 15 µm and 11.12 µm. Testing for the effect of the rake angle on the surface roughness, the calculated p-values are 0.00776 and 0.000325 which suggest that there is an effect due to rake angle. Furthermore, the pairwise-comparison show that only the 10° and 12° rake angles have a difference in R_a and R_z values between them, with adjusted p-values of 0.0053 and 0.000194 respectively. This suggests that the rake angle has no influence on the surface roughness.

Similar analyses were performed to test the effect of preheating on surface roughness. The surface roughness at different temperature is plotted in Fig. 8. The pairwise-comparison test indicates that preheating has no significant effect on the surface roughness, regardless of the temperature.

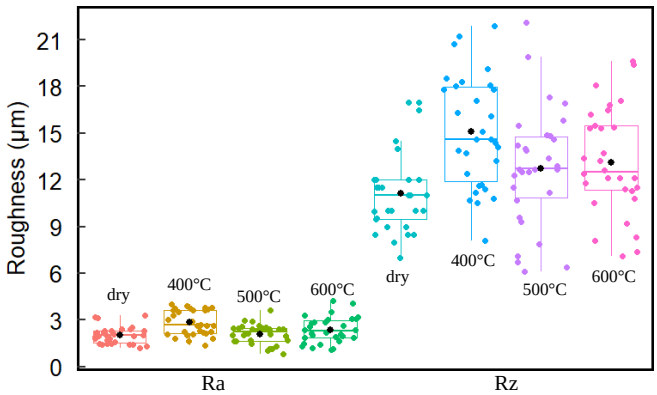

Fig. 8. Surface roughness plots of dry and preheated samples at 400, 500 and 600°C

Optical microscopic observations showed that the machined surfaces contain regions with distinct topographies. Localized 3D topographical contour plots are shown in Fig. 9 and Fig. 10 to reveal the variation across the machined surfaces. Fig. 9 shows the impact of the rake angle while the surfaces in Fig. 10 are due to the cutting speed.

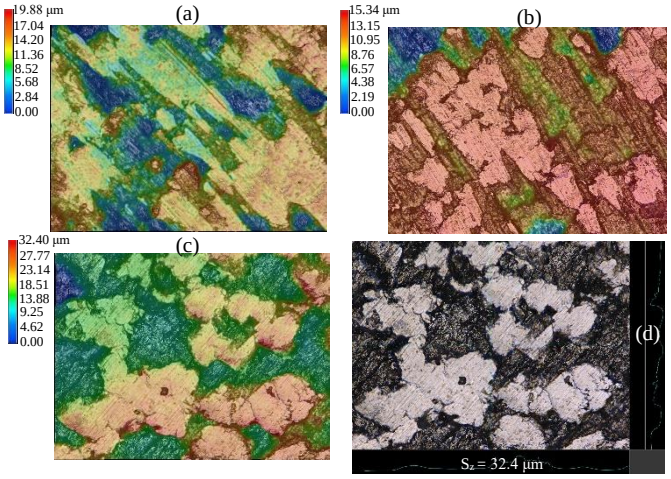

Fig. 9. Surface topographies of machined surfaces at 60 m/min for (a) 8°; (b) 10°; (c) 12°; and (d) typical profile as seen through the microscope

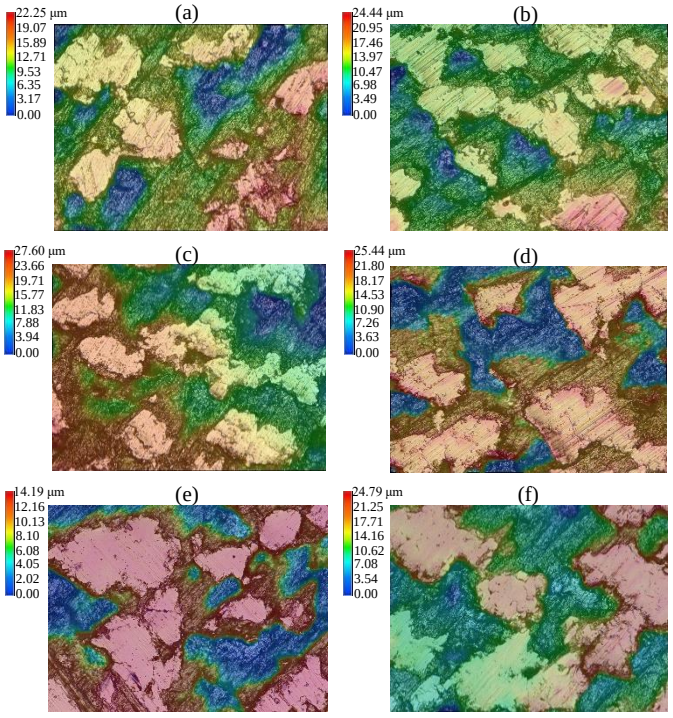

Fig. 10. Surface topographies at different cutting speed for (a) 8° at 100 m/min; (b) 8° at 150m/min; (c) 10° at 100m/min; (d) 10° at 150m/min; (e) 12° at 100 m/min; (f) 12° at 150

The topographically elevated region is seen as “bright” (Fig. 9(d)) due to reflection. This region is typically distributed across the machined surface and is neither concentrated depending on the cutting pass nor affected by the cutting speed or rake geometry as Fig. 9 and Fig. 10 show.

Topographies of the preheated samples at 400 °C, 500 °C and 600 °C are also shown in Fig. 11 and compared to the dry machined sample. This reveals that preheating produced similar features and has no significant effect on the topography. Further [illegible] the preheat[illegible]

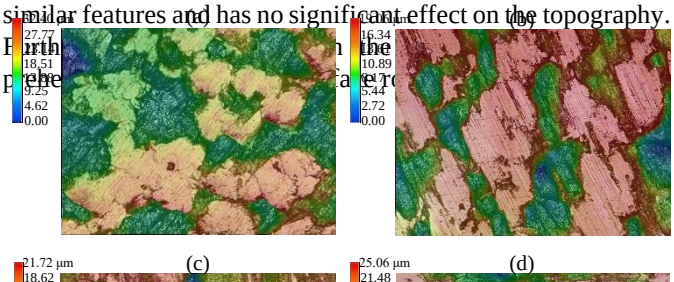

Fig. 11. Surface topographies for (a) dry machined sample; (b) preheated sample at 400 °C; (c) preheated sample at 500 °C; and (d) preheated sample at 600 °C

SEM secondary electron images are shown in Fig. 12 to further characterize the machined surfaces. These surfaces have comparable features, as annotated in Fig. 12(a), and further show the difference in topography. Furthermore, the visually observed "bright" regions in Fig. 9(d) correspond to the plastically deformed region as evident from the elevated topography.

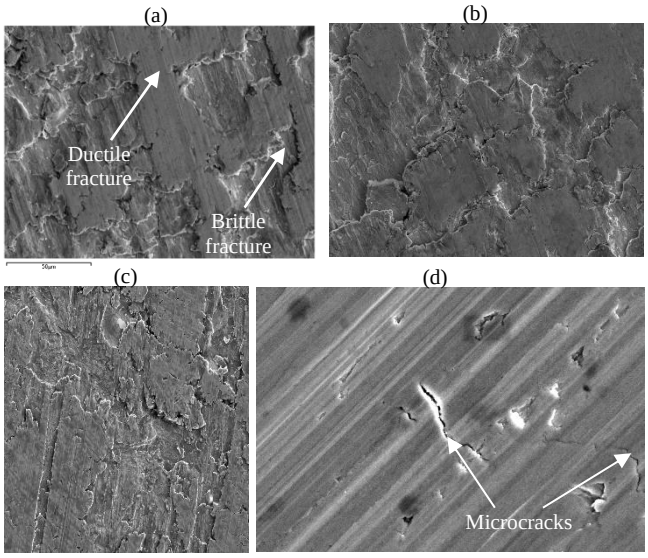

Fig. 12. Micrographs of machined surfaces at 60 m/min for (a) 12°; (b) 10°; (c) 8°; and (d) microcracks within the plastically deformed region

The ductile fracture regions denote the areas where the cutting tool impacts the workpiece and where actual cutting occurred. This is obvious from the cutting marks in Fig. 12(d). Furthermore, the elevated topography of these regions supports the observation that these are areas of actual impact. The brittle regions are due to fracture with no or minimal plastic deformation. These regions serve as evidence of the brittle nature of tungsten and are the main observation of embrittlement that can be made post-machining.

The large areas covered by each brittle fracture region also explain the high surface roughness measured in this study. Hence, improvement in ductility of tungsten can be assessed through analyses of these brittle regions. Reduction in the area covered by these regions will mean improved ductility. Further characterization within the ductile fracture regions shows the presence of microcracks as in Fig. 12(d). These also serve as additional evidence of the brittle nature of the material.

3.3. Subsurface deformation

Subsurface evaluation of the grain structure due to the impact of deformation showed a layer of refined grains closer to the machined surface as in Fig. 13. This refined grain region is equivalent to a hardened layer from the knowledge of the hardness-grain size relation in tungsten and other metals. There is also evidence of cracks within this depth of deformation-induced grain refinement which will require further investigation.

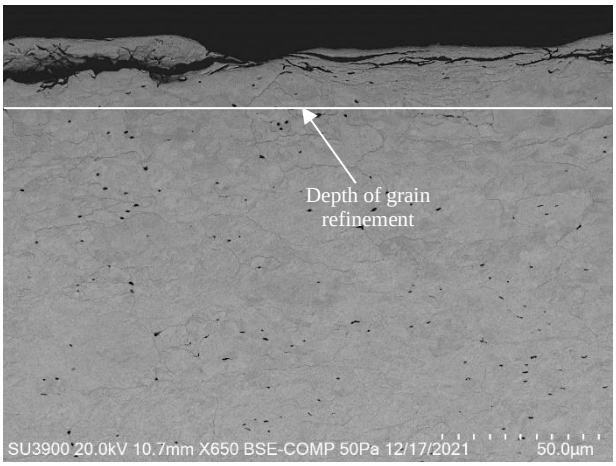

Fig. 13. Backscattered-electron imaging showing deformation-induced refined grains for the sample machined at 60 m/min with the 12° rake angle tool

4. Conclusion

A relatively low cutting speed is required for machining tungsten. A cutting speed of 60 m/min produced the best result in terms of tool life and impact on the workpiece. Findings from this study also suggest a higher a rake angle is required for machining tungsten. The beneficial effect of low cutting speed is more pronounced at higher rake angles. Hence, a combination of higher rake angle and low cutting speed is recommended to achieve improved machinability of tungsten. The tool wear mode is dominated by flank wear and chipping (at the cutting edge and on the secondary flank face). Although the minimum average surface roughness achieved is 2.01 µm for the 12° rake angle at 60 m/min, there is no statistically significant influence of either the rake angle or the cutting speed on the surface roughness. Further observations show the machined surfaces can be characterized as a combination of ductile and brittle fracture regions with microcracks formed within the former.

Improved ductility has been reported in many studies for tungsten when the DBTT is exceeded. However, this study showed that preheating tungsten above the DBTT does not improve machinability. The tool life is shorter and the surface quality is comparable to surfaces produced via dry machining.

While it is possible that the workpiece became ductile, the thermal effect of preheating on the cutting tool is adverse as evidenced by the poor tool performance. This may have combined with the heat generated at the cutting zone to make the temperature reach or exceed the thermal limit of the carbide cutting tool. Observations of the machined surfaces due to preheating also show similar features as dry machined samples.

While a high rake angle is suitable for the milling of tungsten, this study also acknowledges there will be a limit beyond which the benefits diminish. Future investigation will aim to optimize this rake geometry through experiments and supported by a simulation approach. While preheating has proven to be ineffective in this study, it is possible that the cutting parameters (e.g., the radial depth of cut) could have significant influence on outcomes. Further investigation will involve the optimization of cutting parameters to assess the impact of workpiece preheating temperature on machining performance.

Acknowledgements

This work was supported by the UK Atomic Energy Authority with funding from EPSRC Grant EP/T012250/1

References

[1] Y. Ueda *et al.*, “Research status and issues of tungsten plasma facing materials for ITER and beyond,” *Fusion Eng. Des.*, vol. 89, no. 7–8, pp. 901–906, 2014.

[2] M. V. Aguirre, A. Martín, J. Y. Pastor, J. Llorca, M. A. Monge, and R. Pareja, “Mechanical behavior of W-Y2O3 and W-Ti Alloys from 25 °C to 1000 °C,” *Metall. Mater. Trans. A Phys. Metall. Mater. Sci.*, vol. 40, no. 10, pp. 2283–2290, 2009.

[3] L. Zhong, L. Li, X. Wu, and N. He, “Micro cutting of pure tungsten using self-developed polycrystalline diamond slotting tools,” *Int. J. Adv. Manuf. Technol.*, vol. 89, no. 5–8, pp. 2435–2445, 2017.

[4] S. Legutko, P. Winiarski, T. Chwalczuk, L. Marcincinova-Novakova, and K. Zak, “Tool Life of Ceramic Wedges During Precise Turning of Tungsten,” in *MATEC Web of Conferences*, 2017, vol. 94, pp. 1–9.

[5] M. Olsson, V. Bushlya, F. Lenrick, and J. E. Ståhl, “Evaluation of tool wear mechanisms and tool performance in machining single-phase tungsten,” *Int. J. Refract. Met. Hard Mater.*, vol. 94, no. 105379, pp. 1–11, 2021.

[6] M. Olsson, V. Akujärvi, J. E. Ståhl, and V. Bushlya, “Cryogenic and hybrid induction-assisted machining strategies as alternatives for conventional machining of refractory tungsten and niobium,” *Int. J. Refract. Met. Hard Mater.*, vol. 97, no. 105520, pp. 1–14, 2021.